IEEE Access
Multidisciplinary ⋮ Rapid Review ⋮ Open Access Journal

Received 29 November 2022, accepted 15 December 2022, date of publication 19 December 2022,
date of current version 22 December 2022.

Digital Object Identifier 10.1109/ACCESS.2022.3230588

APPLIED RESEARCH

Novel Measurements and Features for the Characterization of Soil Surface Roughness

ANTONIO LEANZA[1], GIOVANNI MATRANGA[2], MARCELLA BIDDOCCU[2], EUGENIO CAVALLO[2], ANNALISA MILELLA[3], AND GIULIO REINA[1]

[1]Department of Mechanics, Mathematics, and Management, Politecnico di Bari, 70126 Bari, Italy
[2]Institute of Sciences and Technologies for Sustainable Energy and Mobility (STEMS), National Research Council of Italy (CNR), 10135 Torino, Italy
[3]Institute of Intelligent Industrial Technologies and Systems for Advanced Manufacturing (STIIMA), National Research Council of Italy (CNR), 70126 Bari, Italy

Corresponding author: Giovanni Matranga (giovanni.matranga@stems.cnr.it)

This work was supported in part by the European Union's Horizon 2020 Research and Innovation Program "ATLAS—Agricultural Interoperability and Analysis System" under Grant 857125; in part by the ERA-NET COFUND ICT AGRIFOOD "ANTONIO-multimodal sensing for individual plANT phenOtyping in agriculture robotics under Grant 41946; in part by the Programma Operativo Nazionale (PON) Agrifood Program, Italian Ministry of University and Research (MUR) "E-crops-Technologies for Digital and Sustainable Agriculture" under Grant ARS01 01136; and in part by the Dipartimento di Ingegneria, ICT e Tecnologie per l'Energia e i Trasporti, Consiglio Nazionale delle Ricerche (CNR-DIITET) Project "DIT.AD022.180 Transizione Industriale e Resilienza delle Società Post-Covid19 (Fondo Ordinario per gli Enti e le istituzioni di ricerca (FOE) 2020)," Sub Task Activity "Agro-Sensing."

ABSTRACT Agricultural soils provide a variety of ecological services, including nutrient cycling, water purification and storage, carbon sequestration, and flood protection. Soil Surface Roughness (SSR) represents a key parameter for evaluating the terrain quality structure, especially in the layers beneath the usual primary tillage depth, and therefore its estimation has been widely investigated over the years in many fields of science and engineering. This paper proposes the adoption of an innovative sensing approach that relies on contactless measurements provided by a depth camera in contrast to traditional contact measurements such as pin meter and roller chain. In addition, novel features are investigated to achieve a complete statistical description of the SSR with the least number of parameters. The proposed methods are validated in an experimental campaign performed on a vineyard plot. This research could be useful for many applications, including soil erosion prediction models, autonomous vehicle navigation in rural and agricultural settings, and controlled traffic farming.

INDEX TERMS Soil surface roughness, vision-based sensing, environmental preservation and monitoring, precision agriculture, intelligent vehicles, agricultural robotic.

I. INTRODUCTION

Nowadays, the concept of sustainability is a paramount issue for socioeconomic perspectives and environmental trouble [1], and affects all the human activities. Among them, the agriculture plays a significant role, involving several key environmental issues, such as water resources, diffusion of chemical plant protection products, soil threat like organic matter reduction, compaction, erosion and so forth [2]. The last soil degradation processes is of particular interest for this research and it is strongly dependent on soil properties, such as moisture, texture, and roughness. The characterization of these properties, especially in a suitable quantitative way, can be meaningful to achieve the sustainability criteria required today. This manuscript focuses on the issue of the Soil Surface Roughness (SSR) evaluation, which is an active area of research with relevance and applications to many fields of sciences and engineering. SSR is an intrinsic feature of soil geometry, which is generally defined as the variation in surface elevations in relation to "zero" asset on different scale terms. M.J. Romkens [3] classifies SSR at 4 scale terms: *a*) Original soil roughness refers to micro-relief variation of soil aggregate on an unaltered terrain, which has a millimeter scale. *b*) Surface variation due to soil alteration by ploughing causing clodiness, the so-called random roughness in centimeter scale. *c*) Oriented roughness (also cm scale) as consequence of soil tillage by farm implements with scissor tools as rippers, weeders and harrows. *d*) Meter scale

The associate editor coordinating the review of this manuscript and approving it for publication was Shaohua Wan.

SSR referring to landscape elevation variation due to hillslopes, depressions, ground cover, basins, etc. In this study, the SSR is referred to as type *b* and *c*.

SSR estimate is important for several agricultural tasks. For instance, they are considered a valuable benchmark for soil management [4] dealing directly with the study of the hydrological behavior on a surface during rainy events. In particular, SSR is one of the key variables in soil erosion prediction models as the Revised Universal Soil Loss Erosion (RUSLE) [5], its derivatives [6] and the LImburg Soil Erosion Model (LISEM) [7]. The capability of managing the soil erosion is fundamental for facing natural disasters, as floods, loss of fertile land, soil degradation, water quality and runoff, which occur when the amount of rain exceeds the infiltration capacity of the soil [8]. The topsoil surface profile in agricultural land is constantly renewed in relation to tillage practices; in fact, high soil surface roughness values are attributable to recently tilled terrain, where disturbed clods form elevations and depressions in surface micro-topography, thus roughness levels change in relation to implement usage and tillage depth conducted in field operations [9]. Conventional soil tillage implies increasing water storage capability, and a reduction of soil loss due to runoff [10]. Indeed, soils where frequent tillage is carried out are characterized by the formation of surface aggregates more sensitive to disintegration by water and wind erodibility [11]. Furthermore, in plain conditions on rougher soil surfaces, rainfall events mobilize soil aggregates, reducing relative roughness, indirectly promoting the phenomenon of raindrop splashing, thus forming crust and sealing the soil [12]. Since the SSR characterizes the shape of any soil surface, they also play a critical role for agricultural vehicle navigation, because they directly affect the dynamic response in terms of vertical vibrations, responsible for human comfort and handling performance, traction and safety, including extreme cases of vehicle entrapment or rollover [13]. Furthermore, new generations of agricultural vehicles [14] need to be sensitive to the SSR in order to achieve an advanced level of autonomous navigation, namely the optimal path planning in terms of traction, travel velocity and safety with less or no human supervision [15], [16], that represents an important challenge for the Agriculture 4.0 [17], [18].

Before dealing with the aims of this study along with the sensors and parameter identification techniques, a brief overview of these aspects is proposed, for the sake of completeness.

The first aspect concerns the measuring tools. Different types have been investigated during the years to gather reliable measurements of terrain roughness. SSR measuring tools can be grouped into two general types [19], [20], [21]. The first one includes contact devices, e.g., pin-meter, roller chain, meshboards and others, characterised by a physical contact between the instrument and soil surface. Contrariwise, the second type incorporates all the devices with no physical contact, as optical sensors, laser-based distance sensors and so forth. To the second group belong the most modern SSR measurement techniques and some of them will be described below, providing some details on how they work, their strength points and drawbacks. Straightforwardly, the contact measuring tools are cheaper but less accurate at the same time. Moreover, they tend to disturb or destroy the surface that is under study. On the other hand, differences exist between the various contactless sensors, in terms of accuracy, cost and ease of use in different scenarios. For example, Synthetic Aperture Radar (SAR) [22] is microwave-based remote sensing [23], which performs well independently of weather conditions, but depends on different instrumental parameters, such as polarization, incidence angle and radar wavelength. Another SSR contactless measuring tool, very used in the field of autonomous vehicle navigation both in on-road and off-road scenarios for hazard detection [24], but also for agricultural terrains characterization [25], is the LiDAR. The acronym means Light Detection And Ranging and it is able to capture a very accurate digitize soil reconstruction with the characterization of millimeter level roughness. However, this technology is rather expensive, although new cheaper LiDARs are now becoming available on the market. Other approaches utilize acoustic backscatter techniques [26] to quantify the SSR on centimeter scales. Stereo and depth cameras represent a good trade-off between strengths and weaknesses of the various systems available nowadays. As a matter of fact, they ensure dense 3D reconstruction at short/medium range with reasonable accuracy, being at the same time more affordable than other systems [13], [25], [27], [28]. It should be also underlined that RGB-D devices lend themselves very well to integration on intelligent robot farmers for high throughput in-field monitoring, leveraging on their compactness and lightness. This is not the case for other more expensive yet accurate sensors such as the CESBIO–ESA laser profiler as in [19]. This sensor is significantly more expensive and requires a dedicated and complex setup that makes it very difficult for practical applications. Instead, in this study the RGB-D Intel RealSense D435 camera has been selected for the experimental measurements, which represents one of the original contributions of this research.

Another novel aspect refers to the proposal of a set of parameters drawing on the statistical distribution of the profile geometry that can be used to complement or replace traditional metrics for the SSR characterization. Standard features and more modern ones can be correlated, identifying the most convenient combination between them, in order to achieve the best SSR description, both qualitatively and quantitatively. By standard SSR parameters, the authors imply the most commonly used indices for roughness characterization, which are normally associated with traditional hydrologic measurement techniques, such as the random roughness [29],the oriented roughness x-y direction [30], the profile index [31], and the tortuosity [32]. In the field of vehicle engineering and robotics, different parameters can be found in the literature. Some examples are Autoregressive Moving Average (ARMA) models [33], polynomial chaos [34], and Power Spectral Density (PSD)-based

approaches that were proposed in previous research by the authors [13], [35] for vehicle ride and traversability purposes. Here, parameters obtained from PSD-based approaches of soil geometry are used for the SSR characterization. The aim of this paper is thus to present a contactless and effective method for qualitative and quantitative characterization of soil roughness, with low money and time effort.

The paper is organized as follows. Section II introduces the measuring devices used in the field and the mathematical tools encountered in this paper, while Section III collects all the results obtained from an experimental survey, along with the experiment setup. Finally, Section IV discusses the results and draws some conclusions.

II. MATERIALS AND METHODS

This section introduces the measuring devices and mathematical tools exploited for the evaluation of the soil surface roughness. First, a thorough description of the specific measurement tools used for data gathering from the investigated terrains is provided. Then, some sets of convenient soil parameters are defined in order to handle the stochastic nature of the data acquired on field.

A. MEASUREMENT TOOLS

As exposed above, different methods have been developed during the years to measure and evaluate SSR. In this research, soil roughness measurement has been acquired both using conventional contact tools, namely the roller chain and the pin meter, and an innovative contactless method, using the RGB-Depth camera Intel RealSense D435. The roller chain is a basic tool consisting of a 1 m long chain, which is located on the soil surface adhering accurately to the soil aggregate, then the chain extremity is measured with a millimeter-graded ruler to have the profile length (Lp) of the transect. The pin meter consists of a horizontal aluminum frame 1 m long, with drill holes 10 mm spaced apart, housing 37 centimeter-graduated aluminum rods 10 mm width. The pin meter frame is positioned perpendicular to the ground and the rods are inserted making them adhere to the soil surface. The data acquired from the pin meter are the elevation values (z) of the rods expressed in cm.

The D435 uses active infrared (IR) stereo technology for depth perception and 3D scene reconstruction. It combines a red/green/blue (RGB) color sensor, an IR projector and a left-right IR stereo pair. The stereo imagers feature a field of view of 87(H) $\times$ 58(V) deg, maximum depth resolution of 1280 $\times$ 720 px, and frame rate up to 90 fps, with an ideal perception range of 0.3 m up to 3 m. The IR stereo stream is spatially calibrated and time synchronized with the color stream provided by a FullHD (1920 $\times$ 1080) CMOS camera, with nominal field of view of 69(H) $\times$ 42(V) deg and 30 fps at full resolution. In this work, only the 3D points returned by the stereo pair are used, without color information; however, future developments may include additional features based on color data. Specifically, the soil surface is reconstructed in XYZ coordinates, where Z corresponds to the elevation of the ground with respect to the camera position. This makes the camera data comparable to the elevations of the pin meter z.

The accuracy of elevations z recorded with both the pin meter and the RGB-D camera has been assessed before collecting measures on field. Pin meter accuracy is defined by the unit of measure of its graduated rods. As described above, the rods of the pin meters are centimeter graduated, implying that the pin meters z accuracy stands at 1 cm. The D435 z accuracy was determined through the image acquisition in standard conditions. As a matter of fact, under the defined camera setup (faithfully reproduced in the in-field experiment), the inaccuracies in the elevation measurements can be defined as the background noise recorded on a flat surface attesting to ± 0.27 cm of standard deviation, which can be referred to as the camera elevation accuracy.

B. IDENTIFICATION OF SOIL SURFACE ROUGHNESS PARAMETERS

Due to their random nature, the level of the SSR can be evaluated only by means of statistical approaches. However, some of them can only provide a qualitative description of the terrain roughness. For instance, with the use of the roller chain method described in Section II-A, a PI chain index can be defined as follows [31]:

$$\mathrm{PI}_{\mathrm{idx}} = \frac{1}{L_p} - 1 \tag{1}$$

returning a non-dimensional index directly related to the level of terrain roughness. This index is achieved with a 1 meter long chain (the 1 at the numerator of Equation (1)) and its projection on the terrain profile L_p. Hence, $\mathrm{PI}_{\mathrm{idx}}$ theoretically spans from 0 to $+\infty$ and the higher its value, the harsher the terrain profile and *vice versa*. Usually, L_p is greater than 0.5 m, therefore the value of $\mathrm{PI}_{\mathrm{idx}}$ is between 0 and 1. However, more efficient indices can be introduced in order to obtain a more representative description of the level of SSR.

By considering a single terrain profile defined as a random function $z = z(s)$, with s the length coordinate and z the profile elevation, its first two statistical moments can be straightforwardly evaluated in order to achieve an early quantitative characterization of the profile roughness. The first statistical moment, namely the profile average, is influenced by the slope of the profile, that in turn can be carefully evaluated by exploiting other methods, such as the first order polynomial regression, therefore it is convenient to discard the slope through a detrending manipulation, which also helps for deleting possible offsets due to the measurement device. After detrending manipulation the resulting average of $z(s)$ is zero. The second statistical moment contains significant information about the amplitude of the roughness associated to the terrain profile, that can be directly achieved whether a null-mean profile is considered. As a matter of fact, the second moment of a zero-mean profile is equal to its second central moment, hence the mean square value and the variance are the same. Therefore, a convenient parameter for

(a)

(b)

(c)

FIGURE 1. Measurement tools utilized in the experiment. The roller chain (a) and the pin meter (b) are the traditional tools for SSR characterization, while the Intel Realsense D435 (c) is the proposed RGB-D camera.

evaluating the level of unevenness of a given (zero-mean) terrain profile is its standard deviation σ_z:

$$\sigma_z = \sqrt{E\left[z^2(s)\right]} \tag{2}$$

where $(E\left[z(s)\right])^2 = 0$. This parameter allows to define an overall level of roughness associated to a specific terrain profile and it is particularly suitable for the classical methods of terrain roughness evaluation, such as the pin meter. Nevertheless, it does not give any further information on the geometry of the terrain profile.

In Figure 2 two different profiles are displayed, sharing the same standard deviation σ_z but having very different shape. In order to achieve a quantitative shape characterization of a given terrain profile, the analysis in the spatial frequency

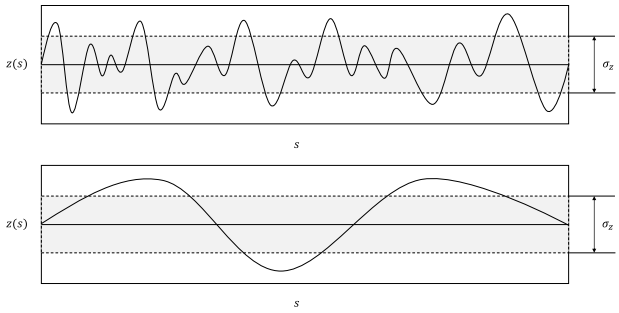

FIGURE 2. Example of profiles with the same σ_z standard deviation but with different geometry.

domain represents a convenient approach. Spatial frequencies are the spatial corresponding of the most common time frequencies, defined as $1/T$, where T is the time period. Similarly, spatial frequencies are defines as $1/\lambda$ with λ the wavelength. The spatial frequencies content of the two profiles depicted in Figure 2 is different and can be appropriately evaluated and even parameterized. Although a generic random profile contains a theoretical infinite number of wavelengths, in practice there is always an upper and lower limit. The longest and shortest profile wavelength are defined by the profile length and twice the value of the spatial sampling frequency, in compliance with the Nyquist-Shannon theorem. Therefore, the waveband of interest is obtained, depending on the sampling frequency and the profile inspection length. Once the spatial waveband has been defined, the next step consists in selecting a convenient tool to capture the spatial frequencies content of the terrain profile. In this research the one-sided Power Spectral Density (PSD) grounded on the Bartlett-Welch method [36] is exploited in order to achieve a quantitative spatial frequency description of the terrain profiles. As an example, Figure 3 shows the PSD (solid grey line) of a generic terrain profile. As seen from this figure, the PSD typically decreases with increasing wavenumber Ω, defined as 2π times the spatial frequency. It is common to approximate the spectral density curve of the terrain profile by an exponential equation, which gives a straight-line fit on a log–log plot of the PSD spatial frequency diagram (solid black line in Figure 3):

$$\hat{\Phi}\left(\Omega\right) = R\Omega^w \tag{3}$$

where w and R are constants that relate, respectively, to the slope and scaling of the fit line $\hat{\Phi}$ and represent a new set of convenient parameters to quantitative describe the spatial frequency content of a generic random terrain profile and then achieving a sort of shape representation of the terrain roughness. From the PSD fit line, completely described by means of these two parameters, it is possible to recover the σ_z by using the following equation [37]:

$$\sigma_z^2 = \int_0^{+\infty} \hat{\Phi}\left(\Omega\right) d\Omega \tag{4}$$

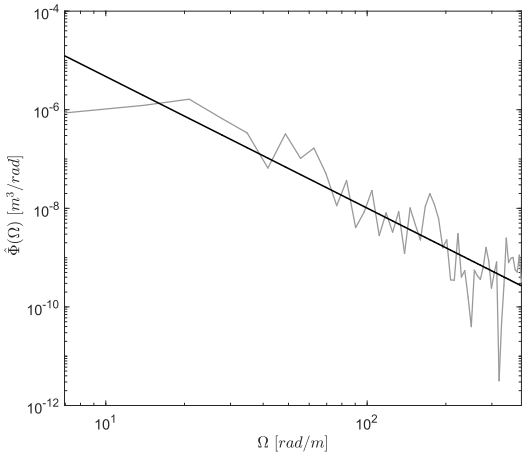

FIGURE 3. Example of profiles with the same σ_z standard deviation but with different geometry.

considering a zero-mean terrain profile. The meaning of Equation (4) is that the area under the PSD line into the waveband of interest is equal to the zero-mean profile variance. Therefore, the greater the area below the PSD line, the harsher the profile. The slope of the PSD line provides insights on how the spatial frequencies are distributed into the waveband: the steeper the line, the more energy is concentrated on low spatial frequencies, meaning that the profile is characterised by unevenness such as bumps or pits, characterised by high amplitude and long wavelength λ. This information is provided by the waviness w and the higher its absolute value, the steeper the PSD line in the log-log diagram. The R parameter poses the PSD line with respect to the ordinates in the log-log plot and by considering the fundamental wavenumber $\Omega_0 = 1$ rad/m. For a given waviness w, the higher the value of R, the harsher the profile because a greater area is under the PSD line.

Summing up, enough information about the overall level of terrain roughness and also about the profile geometry can be achieved by the use of the standard parameter σ_z and the new ones R and w, respectively. Moreover, as stated above, they are tightly connected by Equation (4).

C. COMPARISON OF SSR INDICES

A comparison of SSR indices is pursued, in order to study the reliability of the proposed coefficients, taking into account the overall data acquisition-elaboration efforts, precision and suitability of soil surface characterization and a statistical elaboration, to know the measurement capability for recognizing different theses is undertaken by one-way ANalysis Of VAriance (ANOVA) and the correlation between coefficients.

III. EXPERIMENTAL RESULTS

This section collects experimental results obtained from data collected with the devices described in Section II-A and performed on a suitable test ground. An overview of the experimental environment is provided before dealing with the results achieved in this research.

A. EXPERIMENTAL SETUP

The area selected for the experimental Soil Surface Roughness (SSR) measurements is a viticultural area known as "Alto Monferrato" in north-west Italy. Measurements were collected in February 2022 in three vine rows in which three soil roughness cases were considered: i) Vine row 30 cm ripping with three working tool rippers recently tilled (RT), i.e. the day before the measurements; ii) Vine row 30 cm ripping with three working tool rippers tilled in past (PT), i.e. 114 days before the measurements; iii) Vine row no-till (NT), with a cover crop. These theses are chosen to observe significant differences in SSR by traditional measurements. In particular, low values of SSR are expected in NT, high values are attended in RT, and intermediate values in PT due to rainfall events that cause soil particle mobilization [38]. RT and PT rows present low or no vegetation, NT was characterized by an homogeneous vegetation cover, mainly composed of poaceae and clovers, having regular heights ranged in 3-6 cm height from the ground. Trimmed branches residues are disseminated in every vine rows. In light of the rainfall data collected by an infield site weather station, referring to PT rows were recorded 44 rainfall events occurred from the past tilling until the measurement, with 188 mm of rain in total amount and 18.7 MJ/ha of kinetic rainfall energy. During that time, no particularly intense rain events were recorded that can result in elevated erosive events. The EI_{30} Rainfall Erosivity Index calculated for each rain event revealed low values, unlike a single event where 35.4 mm in 52 hours has fallen with an EI_{30} of 30.9 $\frac{\text{MJ mm}}{\text{ha hr}}$.

For each theses (i.e., terrain types) described above, five 1 meter long patches of soil have been investigated for a total of fifteen terrain instances. Each terrain portion has been acquired by using the D435 camera, mounted on a support and accurately positioned with the optical axis perpendicular to the ground and at a height of 1 m, capturing a large amount of information, such as photos, the point cloud with the RGB content, infrared images and other information. Furthermore, for each patch, surveys with contact instruments, namely the roller chain and the pin meter, have been carried out in order to quantify the level of SSR by referring to reference profiles inside the inspection window. Figure 4 outlines the layout of the frame acquisitions, along with the 90 deg camera positioning and the sampled terrains profile. As shown in the figure, for each terrain portion under investigation, highlighted with a yellow area, two terrain profiles (red lines) have been surveyed always at +10 and +90 cm from the camera support (represented by a rotated green c in the figure), except for the first patch where a further middle line (+50 cm from the support) has been measured. This layout was maintained for all three theses. All the acquisitions have been performed keeping track of the position with respect to every vine row, in order to allow the repeatability of the surveys and a correct matching between camera acquisitions and profile measurements.

Data acquisition with the three different tools described above gets an idea on the effective timing of each

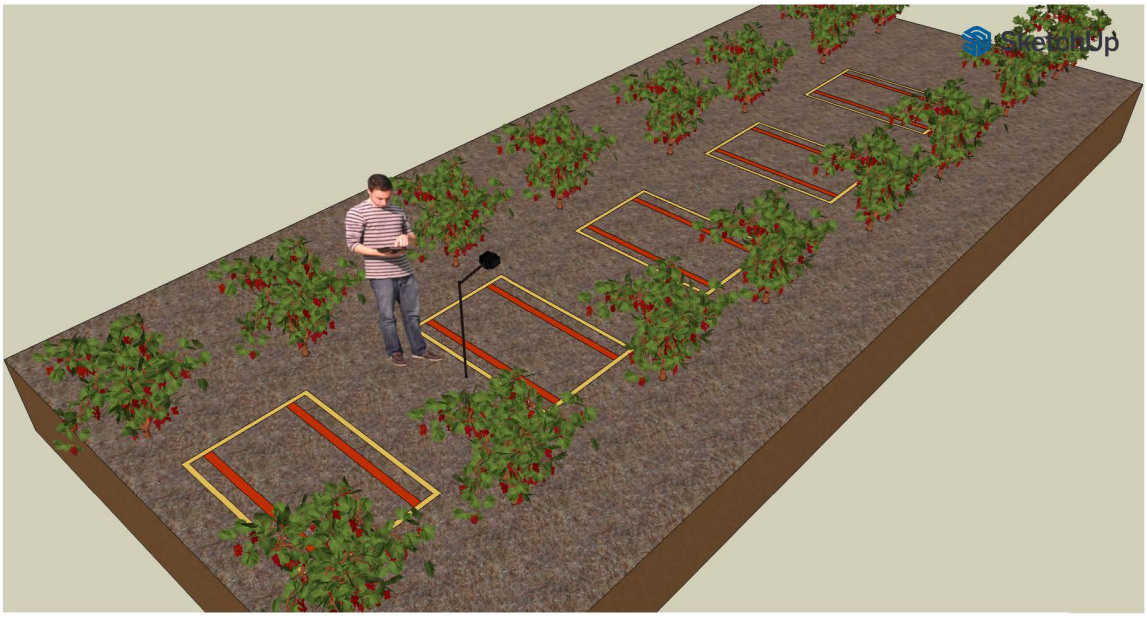

FIGURE 4. Layout of terrain surveys. In yellow the camera acquisition frames, in red the profile sampled with the roller chain and pin meter.

operation execution. Empirical observations demonstrate that one acquisition of pin meter data, consisting of frame settling and leveling, insertion of the graded rods and elevation readings, accounts 15-20 min of operational time, while one acquisition of roller chain profile length takes 1.5 min approximately and finally the camera capture has required about 5 min for support position, camera angle adjustment and take. However, it has to be taken into account the time required for data elaboration: while traditional measurements only need the indirect measure calculation, the RGB-D data need to be extrapolated and elaborated by programming languages before achieving any measurement. Nevertheless, the latter steps can be automated.

Section II-A describes how the devices employed in this research work. However, the acquisitions made with the camera have to be carefully handled, before getting any kind of measurement, in order to achieve an accurate matching between the actual part of terrain under study and the associated point cloud stored in a *.ply* file. One can use the photo captured with the camera for a correct visualization of the associated point cloud by considering some landmarks such as stones, sprigs and so forth. *Matlab* environment includes a dedicated package for managing *.ply* files. This package allows to import and visualize the point cloud gathered by the camera before running any algorithm to obtain the values of soil parameters described in Section II-B. It is worth highlighting that the position of the camera can be automatically estimated by tracking the reference frame with the use of sensors such as IMU. For instance, the D435i is a special version of the D435 camera employed in this research which also includes IMU. D435 camera has a cone of view and then a portion of reliable acquired points that is smaller than the patch length displayed in Figure 4, due to the camera position, height and angle with respect to the ground. In Figure 5 the area of reliable points acquired with the camera and associated to the first patch of the RT soil is displayed, along with the middle profile highlighted in red. This profile has also been sampled with the contact methods, therefore the σ_z value can be achieved both for the profile acquired with the pin meter and that extracted by the point cloud, by considering a strip of 1 cm of width equal to the accuracy of the pin meter device. A very similar value of the standard deviation has been obtained for both methods, ensuring the correctness of the two approaches.

It is worth pointing out that the raw point cloud stored in the *.ply* file is too dense if compared with the accuracy of the contact method (e.g. the pin meter) and moreover the points location is not regular and thus not suitable to manage. Therefore, the point cloud was meshed with a regular-spaced grid with 1 cm step, equal to the accuracy of the pin meter, before applying any algorithm for SSR parameters identification. The grid obtained by meshing the patch depicted in Figure 5a is displayed in Figure 5b. To achieve a more reliable meshed surface, the edges of the patch have been cut before the grid generation to avoid edge effects. The advantage of having a regular meshed surface lies in the ability to slice the patch in several profiles along x or y direction and to perform any patch investigation in a more convenient way. In this research, each profile is intended in the $s = y$ direction, with z its elevation and each realization is with respect to the x direction. Finally, each profile has been detrended prior to analysis for the reasons explained in Section II-B.

B. OUTCOMES

Once the reliability of both the contact and contactless approaches has been guaranteed and after careful data

TABLE 1. Average values of every soil parameters defined in this manuscript with respect to each theses and for each measurement device along with results coming from ANOVA tests.

theses	PI chain		σ_z pin meter [cm]		σ_z D435 [cm]		R [m^3/rad]		w	
RT	0.26	a	3.12	a	3.52	a	0,01754	a	-2,51	a
PT	0.15	b	1.74	b	2.10	b	0,00578	b	-2,51	a
NT	0.05	c	0.54	c	0.90	c	0,00012	c	-1,74	b
sample unit	33		33		894		894		894	
p value	***		***		***		***		***	

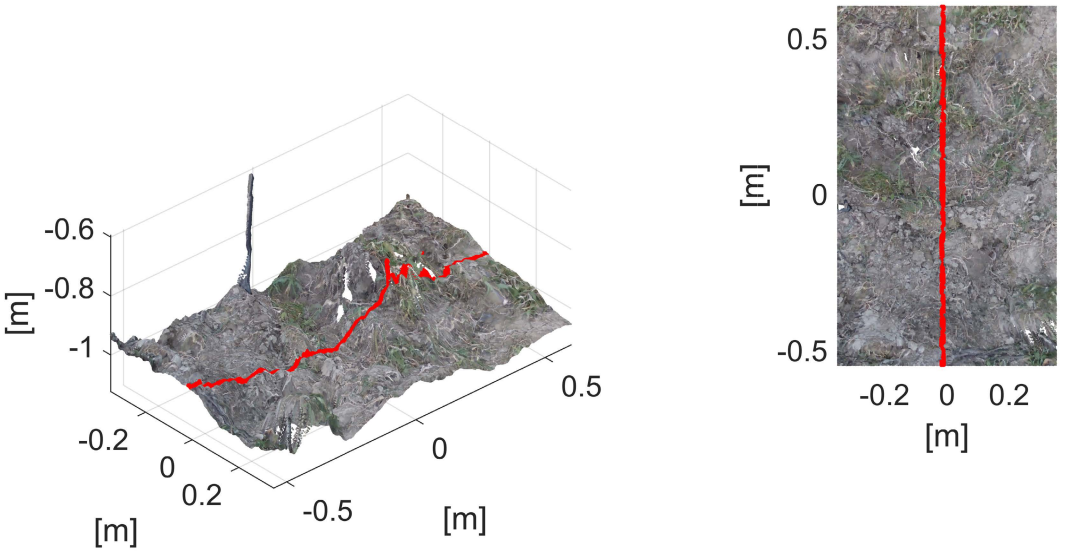

(a) Point cloud captured with the camera, related for the first patch of RT soil. The red profile is that associated to the middle one and also sampled with contact roller chain and pin meter.

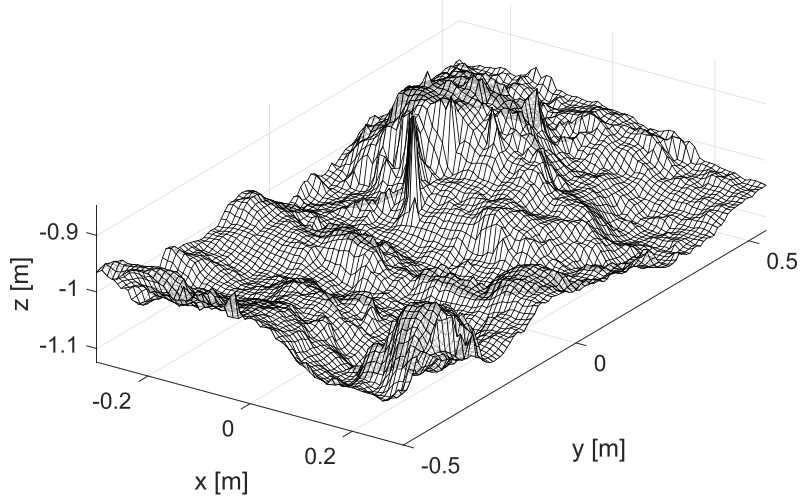

(b) Grid obtained by meshing the first patch of RT soil, with step grid of 1 cm.

FIGURE 5. Raw point cloud (top) a relative grid with regular step grid of 1 cm (bottom), for the first patch of RT.

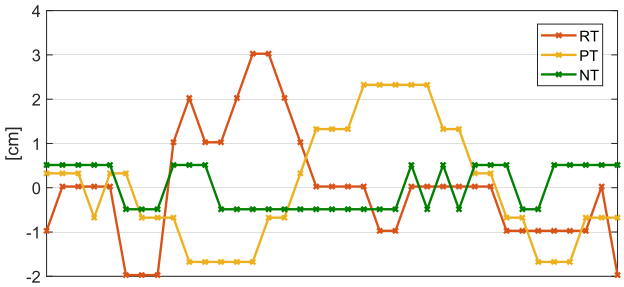

FIGURE 6. Mean profiles obtained by a linear interpolation of the average of measures gathered with pin meter, for each theses.

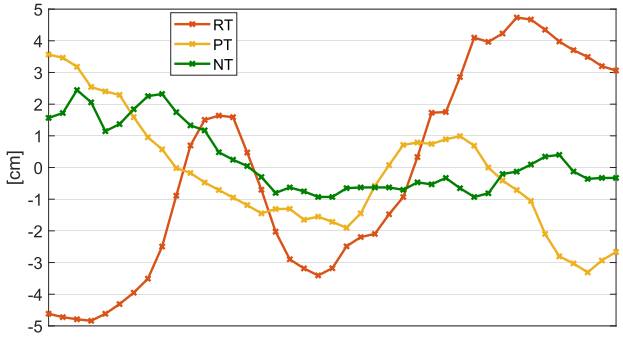

FIGURE 7. Examples of profiles drawn from surfaces acquired with the D435 camera on the three thesis.

pre-processing, several analysis have been performed in order to evaluate the level of SSR of the investigated terrains, the strength points and drawbacks associated to each method and the information carried by each soil parameter defined in this manuscript.

As depicted in Figure 4, 11 profiles have been measured with the contact devices for each theses, for a total of 33 measured terrain profiles. Therefore, a representative value of the SSR parameters related to each kind of terrain can be obtained. 33 measures have been acquired in-field with roller chain, obtaining an average PI_{idx} of 0.26 for the RT soil, followed by a reduction to 0.15 for the PT one and achieving a mean of 0.05 for the No-Tilled soil. 33 profiles have also been measured with the pin meter and the averaged σ_z has been calculated, showing the highest values for the RT (3.12 cm), intermediate values for the PT (1.74 cm) and very low σ_z for the NT (0.05 cm). Figure 6 displays the averaged profiles relative to each theses, obtained by the pin meter measures. The profiles in the figure are achieved by a linear interpolation between a couple of measured points, highlighted with a cross on the profile lines. As one can see, the mean profiles related to RT and PT soil are similar in the shape, but the RT one has a higher amplitude, also confirmed by the value of σ_z, because the PT one has been modelled and smoothed by atmospheric phenomena, such as rain, wind and so forth. Instead, the NT profile is rather flat with an amplitude always less than 1 cm for the considered case.

For the sake of completeness, Figure 7 displays three examples of profiles drawn from one of the surfaces acquired with D435 camera on the three different kinds of terrain. Since the camera is characterized by a higher accuracy with respect to the pin meter, the profiles appear smoother, leading to a more reliable measurements. This aspect represents a very important advantage in the use of the modern vision system technologies in place of the traditional contact

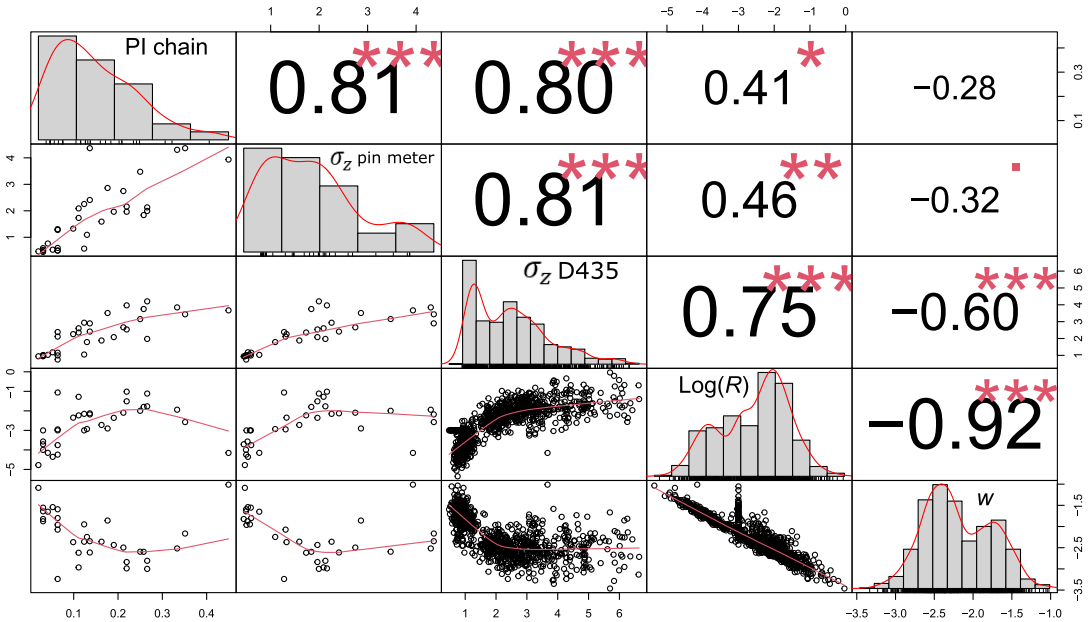

FIGURE 8. Correlation matrix chart of PI_{idx} of the roller chain, σ_z of the pin meter, σ_z of the D435, Log(R), and w SSR measurement values. At the upper part of the graph, the numbers represent the correlation coefficient r, the stars represent the p-value of the correlation (* p<0.05; ** p<0.01; *** p<0.001). The lower part graphically represents the correlation of each variable combination. Diagonal cells show the reference measurement and their histograms. Each cell corresponds to the variables intercepted along their horizontal and vertical axes.

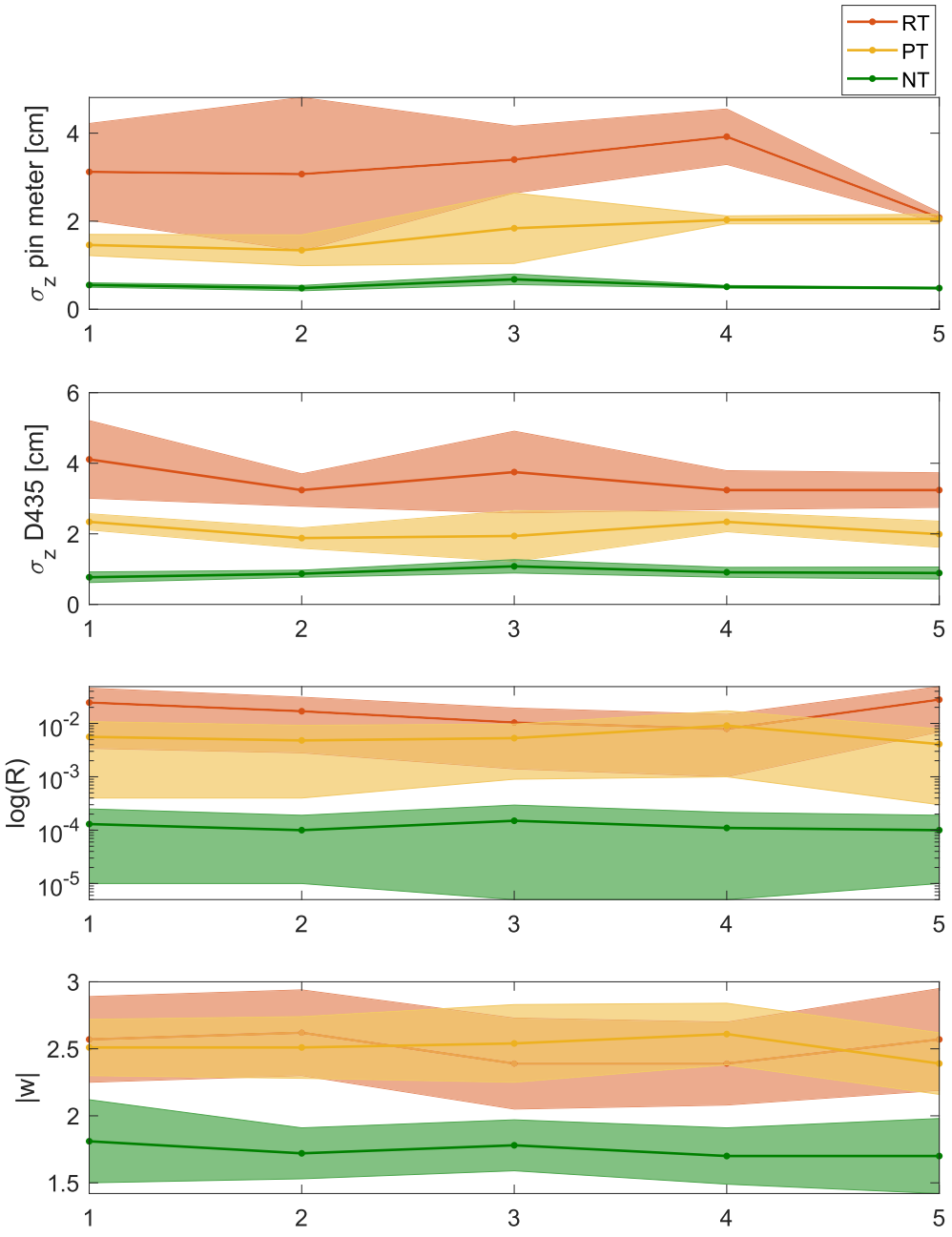

FIGURE 9. Average values and confidence intervals of σ_z relative to pin meter and D435 camera, log of R parameter and waviness w, for every replica of each theses.

devices. Again, the profile lines are obtained by a linear interpolation of the sampled points, highlighted with a cross in the figure.

Table 1 shows the average outcomes of data collected with traditional methods and with the Intel RealSense D435 and processed with Matlab, for each theses. ANOVA tests demonstrated highly significant differences for each indicator, and post-hoc analysis has shown that there are clear differences between the measures for each theses and all indices except for the index w, since no significant differences were found between RT and PT theses. This means that traditional measurements, as well as the proposed indices by RGB-D camera acquisition, give solid information about the surface roughness status of the soil. Another statistical evidence is represented in Figure 8, where the correlation of each measure variable has reported. The analysis show a high statistically significant correlation in almost every combination. The tight correlation ($r = 0.81$) between traditional measurements and σ_z D435 is reported with particular attention, as well as σ_z D435 have close correlation ($r = 0.75$) with R coefficient (or rather its $\log(R)$ transformation), while w parameter doesn't explain soil roughness traditional indices ($r = -0.32$ with σ_z pin meter and $r = -0.28$ with $\mathrm{PI_{idx}}$). The correlation analysis therefore provides indications on the reliability of the

proposed measurements assuming the traditional ones as ground truth.

The quantitative parameters introduced above are displayed in Figure 9, averaged for every replica of each theses. The overall level of SSR indicated by the σ_z parameter is displayed in the two plots on top for measurements obtained with the pin meter and the camera respectively. The results achieved with ANOVA analysis are graphically supported by these two plots, where the three theses are easily distinguishable. A further useful information provided in this figure is the variability associated to every replica of each theses beside the mean value. It has been achieved by performing the standard deviation of the involved parameter (e.g. σ_z for the first two plots on top). As expected, the highest variability in terms of σ_z is obtained for the RT case, because the higher level of terrain unevenness, the more broad their distribution, since the shape of the soil surface can be subjected to abrupt variations in a very small area. A clear example is given by the soil patch displayed in Figure 5, where the profiles at $x \simeq -0.2$ m are clearly very different with respect to those at $x \simeq 0.2$ m, both in geometry and level of roughness. *Vice versa*, the NT theses show the lowest mean values and variability at the same time. The PT behaves between RT and NT, as expected. The two bottom plots display the average value and their interval of confidence for the two features associated to the PSD referred to every replica. For these parameters, the RT and PT cases are less distinguishable, especially by looking at the waviness w. Although the mean value of R is enough different for these two cases, it is strongly influenced by the waviness, as shown in the correlation matrix depicted in Figure 8, leading to an intersection of boundaries relative to these two theses. The NT soil continue to behave very different, instead. The lack of a clear distinction of the RT and PT especially with respect to w parameter means that they show a very similar surface shape, but with different level of height as provided by the σ_z parameter and as shown by the mean profiles displayed in Figure 6. Contrariwise, the shape of the NT theses is quite different and more "regular" because a lower level of $|w|$ means an absence of soil unevenness with high amplitude like bumps or pits. In short, with a simple glace, these plots allow a high comprehension on how the level and the shape of the SSR characterise each theses.

IV. DISCUSSION AND CONCLUSION

This paper investigates novel methods to evaluate the soil surface roughness. First, traditional and new devices have been compared, with a focus on the two contact methods based on the roller chain and the pin meter along with an innovative approach to the contactless vision system represented by the Intel RealSense RGB-D D435 camera. Then, different parameters have been defined in order to quantify the overall level of terrain roughness and how discontinuities are distributed among the spatial frequencies to achieve an adequate representation of their shape. The consistency of the measurements collected by the involved devices, especially by the pin meter and the D435 camera, has been guaranteed by the value of the standard deviation σ_z associated to each theses, that is very similar if computed from pin meter measures or camera acquisitions and processing. The SSR results reported are not directly comparable with the literature as they are closely correlated with the tool used and the depth of tillage. However, the range of values are in good agreement with similar studies [9], [39]. Herodowicz-Mleczak et al. [40] calculated a mean Height Standard Deviation (HSD) of 30.9 mm for soil plowed, using raster-vector calculation algorithm from DEM obtained by photogrammetric images.Values obtained for σ_z for RT (soil recently tilled) with the three methods are consistent with initial roughness value indicated in the RUSLE2 database for subsoiler (Ra $=$ 1.2 inches $=$ 30.48 mm) [41], [42].

There are several advantages in using the proposed vision-based contactless approach.

- First, the profiles are not modified by the measurement device, whereas contact methods involve touching the terrain, thus slightly influencing its shape.
- More information can be captured and in a shorter time. As a matter of fact, the camera is able to acquire an entire patch of terrain composed of different profiles, instead the traditional methods like the roller chain or the pin meter can capture only a profile per time. Moreover, their positioning and measure taking is more time consuming, less practical and can not be automatized.
- Contactless vision systems are characterized by higher accuracy than traditional contact methods.
- Devices like the camera used in this research can be mounted on autonomous systems and the level of the SSR can be automatically evaluated for different tasks characterized by very high technological content.

One limitation of the proposed estimation approach lies in its intrinsic contactless nature. Poor measurements can be expected in the case of physical obstacles between the camera and the soil surface, including low vegetation covering the vineyard soil [20]. As a result, the acquisition of soil surface roughness data through contactless tools must be carried out in conditions of predominantly bare terrain or with a uniform and recently regulated ground cover through cutting tools. Two conditions that are often verified in the field due to the requirement of constant maintenance of the ground cover or the tillage of the soil which eliminates the presence of weeds.

The SSR parameters defined in this manuscript provide information not only on the surface unevenness amplitude, but also on its shape. A convenient set can be selected to get a complete SSR description with a number of parameters as small as possible. For instance, the value of σ_z provide the overall level of the SSR amplitude and the value of w gives information on their shape. Therefore, a full description of their amplitude and geometry can be achieved with only two parameters among those defined in this paper. This pair of parameters is particularly suggested by the authors, but different combinations can be selected. For instance, the two features coming from the PSD-based approach, namely the R and w, with the R in place of the σ_z for describing the overall

level of the SSR can be chosen. Nevertheless, this selection may be less convenient, because the σ_z provides a direct value of the SSR amplitude, instead R is strongly influenced by the waviness w, as shown in the correlation matrix chart in Figure 8 and hence it may assume very different values for a given SSR amplitude when the area underlying the PSD line in the waveband of interest is preserved (see Section II-B). Herodowicz-Mleczak et al. [40] also recently pointed out the needing of a quantitative description of the soil surface roughness. They analysed two of the most used indexes (HDS, height standard deviation) and T3D (tortuosity index), which provide different information about soil roughness, with HSD describing the soil surface roughness on the ''macro'' scale, and T3D at the ''micro'' scale. The results of the present study are in agreement with results of Herodowicz-Mleczak et al., that concluded that a single index, namely HSD, is not sufficient to describe the surface roughness of a post-treatment soil.

RGB-D camera depth information has been shown to be highly reliable and statistical analysis determined high correlation between traditional and new measures. This study highlighted the strengths of the measures proposed for soil surface characterization: in comparison with further contactless technologies able to collect soil surface elevation and other information as the roughness, e.g. Digital Elevation Models (DEMs) by terrestrial LiDAR [43], the RGB-D camera used in this study is more affordable and easy-to-use device, that gives back on the soil surface micro-topography information with successful accuracy compared to more sophisticated and expensive technologies. This study proposes further indices capable of providing more information on soil micro-topography. Nevertheless, coefficient w is unable to appreciate substantial differences between RT and PT, due to the fact that these two theses share the same profile geometry, as also appear in Figure 6 and 7. Besides, PT soils can be considered as the same thesis of RT, where the same soil tillage was performed but 114 days before, thus water erosion has just begun the process of particle mobilization and soiling, and consequently only the decrease in sods elevation is notable.

The information provided by an in-depth knowledge of the SSR both in terms of amplitude and shape can be very useful for many agricultural applications, especially in the context of Agriculture 4.0. This advantage increases whether this information is captured and elaborated automatically. The applicability of RGB-D camera for hydrological and agricultural reasons is multiple. In first instance, SSR information is a required measurement for RUSLE calculation, especially in C factor (Land-cover management factor) where SSR is related to tillage practices. The great advantage of RGB-D technology is to obtain up-to-date information on the SSR even following erosive events. The RUSLE model would therefore benefit from more accurate and realistic data associated to a wide range of soil tools and management options. Modelling is not only aimed to soil erosion. As an example, Prasad Gimire et al. [44] used the FASTR overland flow model to demonstrate how surface micro-topography, namely soil surface roughness, affects the hydrological connectivity and therefore the risk of overland flow in relatively flat agricultural fields, with implications for irrigation management. Another virtuous use of 3D acquisition on extensive terrain surfaces is to detect possible preferential path for overland water flow by rill erosion, which, depending on slopes and rainfall intensity, can significantly increase soil loss [45]. Rapid and effective assessment of soil surface roughness would be useful to assess the susceptibility of a soil to produce runoff and sediment yield, which are affected by the adopted tillage practices with a relevant multi-scale temporal, and spatial, variation [46]. To identify possible critical situation in time, means to prevent by adopting good practices in soil management. A further strength of camera usage for agricultural applications is its portability: with due adjustments, the camera can be mounted on farm tractors frequently used during field operations and SSR acquisition can be achieved simultaneously. This proposed device would therefore become a local-specific monitoring tool for soil condition, to be integrated with other automatically acquired data such as weather stations and soil moisture sensors.

Many applications can take benefit from the parameters proposed in this study. A good example is provided by the autonomous navigation of Unmanned Ground Vehicles (UGVs) for agricultural tasks. The knowledge of the amplitude and geometry of the SSR leads to several useful results. An agricultural autonomous vehicle equipped with this kind of technology and intelligence can make decision about the optimal path in terms of trajectory, traction and travel velocity by itself, with less or even no human supervision. Furthermore, in the context of the big data, a huge number of sampled agricultural SSR can provide useful information for a correct design of the vehicle suspension systems to enhance traction, human safety and vehicle manoeuvrability especially for off-road scenarios, like the agricultural environments.

Encouraged by the results obtained in this research, in the next future the authors undertake to develop novel measurement approaches and features selection for soil surface roughness characterization, in order to achieve an ever higher level of knowledge and capacity to distinguish different kinds of terrain, for the manifold advantages reached in several agricultural aspects.

DECLARATION OF COMPETING INTEREST

The authors declare that they have no known competing financial interests or personal relationships that could have appeared to influence the work reported in this paper.

REFERENCES

[1] P. Condrea and I. Bostan, ''Environmental issues from an economic perspective,'' *Environ. Eng. Manage. J.*, vol. 7, no. 6, pp. 843–849, 2008.

[2] T. Vanwalleghem, J. A. Gómez, J. I. Amate, M. G. de Molina, K. Vanderlinden, G. Guzmán, A. Laguna, and J. V. Giráldez, ''Impact of historical land use and soil management change on soil erosion and agricultural sustainability during the anthropocene,'' *Anthropocene*, vol. 17, pp. 13–29, Mar. 2017.

[3] M. J. Romkens and J. Y. Wang, "Effect of tillage on surface roughness," *Trans. ASAE*, vol. 29, no. 2, pp. 429–433, 1986.
[4] T. Bauer, P. Strauss, M. Grims, E. Kamptner, R. Mansberger, and H. Spiegel, "Long-term agricultural management effects on surface roughness and consolidation of soils," *Soil Tillage Res.*, vol. 151, pp. 28–38, Aug. 2015.
[5] K. E. Spaeth, F. B. Pierson, M. A. Weltz, and W. H. Blackburn, "Evaluation of USLE and RUSLE estimated soil loss on rangeland," *J. Range Manage.*, vol. 56, no. 3, p. 234, May 2003.
[6] M. Biddoccu, G. Guzmán, G. Capello, T. Thielke, P. Strauss, S. Winter, J. G. Zaller, A. Nicolai, D. Cluzeau, D. Popescu, C. Bunea, A. Hoble, E. Cavallo, and J. A. Gómez, "Evaluation of soil erosion risk and identification of soil cover and management factor (C) for RUSLE in European vineyards with different soil management," *Int. Soil Water Conservation Res.*, vol. 8, no. 4, pp. 337–353, Dec. 2020.
[7] N. H. D. T. Cremers, P. M. Van Dijk, A. P. J. D. Roo, and M. A. Verzandvoort, "Spatial and temporal variability of soil surface roughness and the application in hydrological and soil erosion modelling," *Hydrolog. Processes*, vol. 10, no. 8, pp. 1035–1047, Aug. 1996.
[8] Y. L. Bissonnais, "Experimental study and modelling of soil surface crusting processes," *Catena, Suppl.*, vol. 17, pp. 13–28, Jan. 1990.
[9] R. G. Moreno, M. C. D. Álvarez, A. T. Alonso, S. Barrington, and A. S. Requejo, "Tillage and soil type effects on soil surface roughness at semiarid climatic conditions," *Soil Tillage Res.*, vol. 98, no. 1, pp. 35–44, Jan. 2008.
[10] E. J. Mwendera and J. Feyen, "Effects of tillage and rainfall on soil surface roughness and properties," *Soil Technol.*, vol. 7, no. 1, pp. 93–103, Apr. 1994.
[11] H. Blanco-Canqui, M. M. Mikha, J. G. Benjamin, L. R. Stone, A. J. Schlegel, D. J. Lyon, M. F. Vigil, and P. W. Stahlman, "Regional study of no-till impacts on near-surface aggregate properties that influence soil erodibility," *Soil Sci. Soc. Amer. J.*, vol. 73, no. 4, pp. 1361–1368, Jul. 2009.
[12] G. Ma, G. Li, X. Mu, W. Hou, Y. Ren, and M. Yang, "Effect of raindrop splashes on topsoil structure and infiltration characteristics," *CATENA*, vol. 212, May 2022, Art. no. 106040.
[13] G. Reina, A. Leanza, A. Milella, and A. Messina, "Mind the ground: A power spectral density-based estimator for all-terrain rovers," *Measurement*, vol. 151, Feb. 2020, Art. no. 107136.
[14] P. Papadakis, "Terrain traversability analysis methods for unmanned ground vehicles: A survey," *Eng. Appl. Artif. Intell.*, vol. 26, no. 4, pp. 1373–1385, 2013.
[15] G. Reina, A. Milella, and R. Galati, "Terrain assessment for precision agriculture using vehicle dynamic modelling," *Biosyst. Eng.*, vol. 162, pp. 124–139, Oct. 2017.
[16] G. Reina, A. Leanza, and A. Messina, "Terrain estimation via vehicle vibration measurement and cubature Kalman filtering," *J. Vibrat. Control*, vol. 26, nos. 11–12, pp. 885–898, Jun. 2020.
[17] Z. Zhai, J. F. Martínez, V. Beltran, and N. L. Martínez, "Decision support systems for agriculture 4.0: Survey and challenges," *Comput. Electron. Agricult.*, vol. 170, Mar. 2020, Art. no. 105256.
[18] S. O. Araújo, R. S. Peres, J. Barata, F. Lidon, and J. C. Ramalho, "Characterising the agriculture 4.0 landscape—Emerging trends, challenges and opportunities," *Agronomy*, vol. 11, no. 4, p. 667, 2021.
[19] F. Mattia, M. W. Davidson, T. L. Toan, C. M. D'Haese, N. E. Verhoest, A. M. Gatti, and M. Borgeaud, "A comparison between soil roughness statistics used in surface scattering models derived from mechanical and laser profilers," *IEEE Trans. Geosci. Remote Sens.*, vol. 41, no. 7, pp. 1659–1671, Jul. 2003.
[20] L. M. Thomsen, J. E. M. Baartman, R. J. Barneveld, T. Starkloff, and J. Stolte, "Soil surface roughness: Comparing old and new measuring methods and application in a soil erosion model," *Soil*, vol. 1, no. 1, pp. 399–410, 2015.
[21] A. Milella, G. Reina, and M. Nielsen, "A multi-sensor robotic platform for ground mapping and estimation beyond the visible spectrum," *Precis. Agricult.*, vol. 20, no. 2, pp. 423–444, 2019.
[22] M. Choke, "Estimation of surface roughness over bare agricultural soil from Sentinel-1 data," Ph.D. thesis, Univ. de Montpellier, AgroParisTech, Paris, France, 2018.
[23] F. T. Ulaby, P. P. Batlivala, and M. C. Dobson, "Microwave backscatter dependence on surface roughness, soil moisture, and soil texture: Part I-bare soil," *IEEE Trans. Geosci. Electron.*, vol. GE-16, no. 4, pp. 286–295, Oct. 1978.
[24] S. Thrun, "Stanley: The robot that won the DARPA grand challenge," *J. Field Robot.*, vol. 23, no. 9, pp. 661–692, 2006.
[25] J. C. Fernandez-Diaz, *Characterization of Surface Roughness of Bare Agricultural Soils Using LiDAR*. Gainesville, FL, USA: Univ. Florida, 2010.
[26] M. L. Oelze, J. M. Sabatier, and R. Raspet, "Roughness measurements of soil surfaces by acoustic backscatter," *Soil Sci. Soc. Amer. J.*, vol. 67, no. 1, pp. 241–250, Jan. 2003.
[27] M. Zribi, V. Ciarletti, O. Taconet, P. Boissard, M. Chapron, and B. Rabin, "Backscattering on soil structure described by plane facets," *Int. J. Remote Sens.*, vol. 21, no. 1, pp. 137–153, Jan. 2000.
[28] M. Trosin, I. Dekemati, and I. Szabó, "Measuring soil surface roughness with the RealSense D435i," *Acta Polytechnica Hungarica*, vol. 18, no. 6, pp. 141–155, 2021.
[29] K. G. Renard, G. Foster, G. Weesies, D. McCool, and D. Yoder, "Predicting soil erosion by water: A guide to conservation planning with the revised universal soil loss equation (rusle)," *Agricult. handbook*, vol. 703, p. 23, 1996.
[30] O. Taconet and V. Ciarletti, "Estimating soil roughness indices on a ridge-and-furrow surface using stereo photogrammetry," *Soil Tillage Res.*, vol. 93, no. 1, pp. 64–76, Mar. 2007.
[31] W. Jester and A. Klik, "Soil surface roughness measurement—Methods, applicability, and surface representation," *CATENA*, vol. 64, nos. 2–3, pp. 174–192, Dec. 2005.
[32] K. Helming, "Die Bedeutung des Mikroreliefs Für Die Regentropfenerosion," Ph.D. thesis, TU Berlin. Bodenökolgie und Bodengenese, 1992, vol. 7.
[33] L. Li and C. Sandu, "Modeling and simulation of 2D ARMA terrain models for vehicle dynamics applications," in *Proc. SAE Tech. Paper Ser.*, Apr. 2007, pp. 1–9.
[34] L. Li and C. Sandu, "Modeling of 1-D and 2-D terrain profiles using a polynomial chaos approach," in *Proc. 16th Int. Conf. Int. Soc. Terrain-Vehicle Syst. (ISTVS)*, 2012.
[35] G. Reina, A. Leanza, and A. Messina, "On the vibration analysis of off-road vehicles: Influence of terrain deformation and irregularity," *J. Vibrat. Control*, vol. 24, no. 22, pp. 5418–5436, Nov. 2018.
[36] J. G. Proakis," *Digital Signal Processing: Principles Algorithms and Applications*. London, U.K.: Pearson, 2001.
[37] G. Rill, *Road Vehicle Dynamics: Fundamentals and Modeling*. Boca Raton, FL, USA: CRC Press, 2011.
[38] Z.-C. Zheng, S.-Q. He, and F.-Q. Wu, "Changes of soil surface roughness under water erosion process," *Hydrolog. Processes*, vol. 28, no. 12, pp. 3919–3929, Jun. 2014.
[39] R. G. Moreno, A. S. Requejo, A. M. T. Alonso, S. Barrington, and M. C. Díaz, "Shadow analysis: A method for measuring soil surface roughness," *Geoderma*, vol. 146, nos. 1–2, pp. 201–208, Jul. 2008.
[40] K. Herodowicz-Mleczak, J. Piekarczyk, C. Kaźmierowski, J. Nowosad, and M. Mleczak, "Estimating soil surface roughness with models based on the information about tillage practises and soil parameters," *J. Adv. Model. Earth Syst.*, vol. 14, no. 3, Mar. 2022, Art. no. e2021MS002578.
[41] *Revised Universal Soil Loss Equation, Version 2 (Rusle2) Official NRCS Database*, USDA NRCS, Washington, DC, USA, 2012.
[42] S. M. Dabney, D. C. Yoder, and D. A. N. Vieira, "The application of the revised universal soil loss equation, version 2, to evaluate the impacts of alternative climate change scenarios on runoff and sediment yield," *J. Soil Water Conservation*, vol. 67, no. 5, pp. 343–353, Sep. 2012.
[43] L. Li, M. A. Nearing, M. H. Nichols, V. O. Polyakov, D. P. Guertin, and M. L. Cavanaugh, "The effects of DEM interpolation on quantifying soil surface roughness using terrestrial LiDAR," *Soil Tillage Res.*, vol. 198, Apr. 2020, Art. no. 104520.
[44] C. P. Ghimire, W. M. Appels, L. Grundy, W. Ritchie, S. Bradley, and V. Snow, "Towards predicting the initiation of overland flow from relatively flat agricultural fields using surface water coverage," *J. Hydrol.*, vol. 596, May 2021, Art. no. 126125.
[45] J. Han, W. Ge, Z. Hei, C. Cong, C. Ma, M. Xie, B. Liu, W. Feng, F. Wang, and J. Jiao, "Agricultural land use and management weaken the soil erosion induced by extreme rainstorms," *Agricult., Ecosyst. Environ.*, vol. 301, Oct. 2020, Art. no. 107047.
[46] J. Luo, N. Wang, Z. Zheng, T. Li, S. He, and P. Tarolli, "Tillage-induced microtopography alters time-dependent intrinsic correlation of runoff and sediment yield," *Soil Tillage Res.*, vol. 221, Jul. 2022, Art. no. 105423.

Open Access funding provided by 'Consiglio Nazionale delle Ricerche-CARI-CARE' within the CRUI CARE Agreement